Texture and Microstructure After Roll-Bonding of an Fe-Al Multilaminate

Guillaume Hanon[1(✉)], Loïc Malet[2], and Laurent Delannay[1]

[1] iMMC, UCLouvain, 1348 Louvain-la-Neuve, Belgium
{guillaume.hanon,laurent.delannay}@uclouvain.be
[2] 4MAT, Université Libre de Bruxelles, 1050 Bruxelles, Belgium
loic.malet@ulb.be

Abstract. A 5-layer laminate composite was produced by roll-bonding at room temperature of a stacking of ARMCO steel and commercial purity aluminum alloy (AA1050). The large rolling draught led to heterogeneous deformation across the thickness of the layered aggregate, which was investigated using finite element modeling. The evolution of microstructure and crystallographic texture was probed using EBSD. Intense localized shear inside the AA1050 layers gave rise to continuous recrystallization, whereas a rolling texture developed in the adjacent iron layer. Both were reproduced using crystal plasticity modeling.

Keywords: Crystal plasticity · Laminate composite · Finite elements

1 Introduction

Roll bonding of metal sheets with contrasted mechanical properties may result in high-performance layered composites e.g. [1,2]. The plastic anisotropy of such composite metal sheet depends on the crystallographic texture development of its constituents, which in turn is influenced by internal stresses building up due to the prescribed co-deformation of adjacent layers [1]. The roll-bonding process typically requires a large reduction (∼50%) of the sheet thicknesses in a single rolling pass, thus involving significant microstructural changes.

If the diameter of the rolls is either much smaller or much larger than the sheet thickness, the rolled sheet undergoes heterogeneous deformation even if it is made of a single material. Both the roll-gap geometry and the friction of the sheet with the rolls may give rise to significant shear parallel to the rolling plane, resulting in a gradient of texture across the sheet thickness [3–8]. The deformation process fulfils orthotropic symmetry only along the sheet mid-thickness

The present work investigates across-the-thickness strain heterogeneity within roll-bonded multi-laminates made of commercially pure iron and aluminium. The preparation of samples and their characterisation via EBSD are presented in Sect. 2. Experimental observations are then compared to numerical simulations. This involves both the finite element modelling of a rolling pass and

K. Mocellin et al. (Eds.): ICTP 2023, LNME, pp. 646–653, 2024.
https://doi.org/10.1007/978-3-031-40920-2_67

crystal plasticity predictions of the texture development (Sect. 3). Results are discussed before reaching the conclusion.

2 Preparation and Characterisation of Roll-Bonded Samples

Two common metal grades were selected for the present work. With a yield stress of 75 MPa and a UTS of 120 MPa the 1050 aluminium alloy sheets were about three times softer than the sheets made of ARMCO steel ($\sigma_{yield} = 250$ MPa and $\sigma_{UTS} = 300$ MPa). Before being stacked and roll-bonded, both metals had equiaxed grains and a very weak crystallographic textures.

The roll-bonding proceeded in two steps, using a laboratory cold-rolling mill. The diameter of the rolls was 112 mm. The first rolling pass was applied to a stacking of two 0.4 mm-thick AA1050 sheets separated by a single 0.8 mm-thick iron sheet. The total thickness was reduced to 0.62 mm, which corresponds to 61% thickness reduction. Then, two 0.2 mm-thick iron layers were added on either side of the 3-layer composite sheet. The second rolling pass reduced the total thickness to 0.62 mm, which corresponds to an extra 39% thickness reduction.

All to-be-bonded surfaces were preliminary degreased in Acetone and brushed with a 0.3 mm diameter wire-brush in order to remove a the oxide layer. Between the two rolling passes, the 3-layer composite was held at 500 °C during 30 min, which allowed annealing the AA1050 sheet.

Due to the strength contrast, it was a real challenge to prevent relative motion of the sheets at the entrance of the roll gap. Successful bonding was achieved by preliminary folding of the AA1050 sheet around the iron (pass 1) or the iron sheet around the three-layer stacking (pass 2). Figure 1 illustrates the successive folding steps before pass 1.

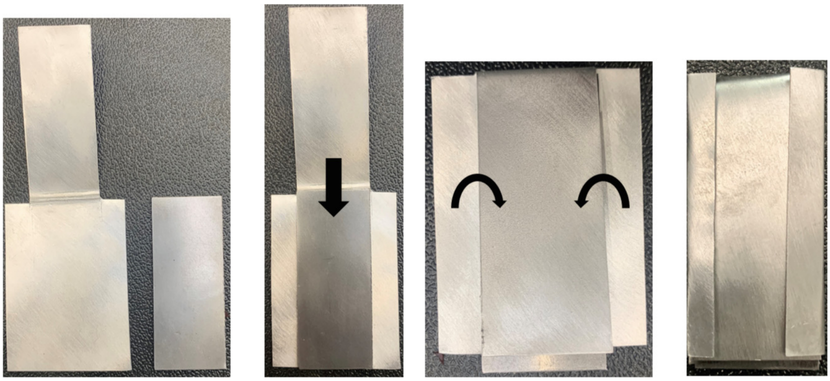

Fig. 1. Before the first rolling pass, the aluminium sheet is folded around the iron sheet to prevent relative motion, which would impede bonding.

Optical microscopy observation of the sheet longitudinal cross-section (Fig. 2) confirmed balanced co-deformation of the two metals and uniform thickness reduction in all layers. A thin oxide film at the interface (not fully eliminated after the inter-pass heating) did not impede successful bonding.

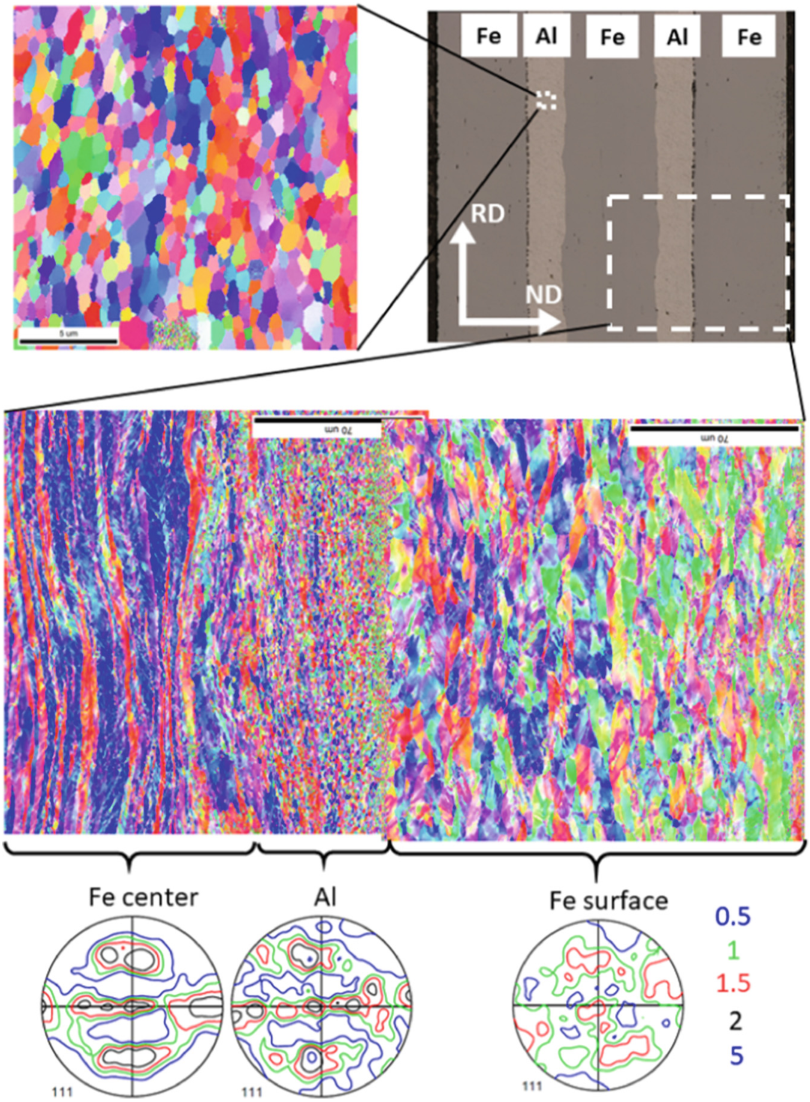

Fig. 2. Microstructural characterization based on optical microscopy and EBSD. The coloring of orientation maps is according to the ND-IPF. The ⟨111⟩ pole figures show the textures developed in the Fe and AA1050 layers.

The crystallographic texture was probed within each layer using electron back scatter diffraction (EBSD). This required prior polishing using SiC up to grid 1200 followed by diamond suspension up to 1 μ and OPS. The orientation maps are colored according to the inverse pole figure (IPF) of the normal to the rolling plane (ND). The iron layer located at the sheet mid-thickness (left on the figure) shows elongated grains and a texture which is typical of cold rolling. The pole figure of the external layer made of iron does not show a clear texture. This layer was added after the first rolling pass and it was hence less deformed than the central layers. The aluminum layer shows a refined equiaxed microstructure. The high indexation rate in the close-up EBSD scan is indicative of continuous recrystallization [9].

3 Numerical Modeling

Finite element modeling allowed simulating the heterogeneous deformation of the sheets inside the roll gap. The Abaqus/Standard (*d'Assault Systèmes*, France) commercial code was used. As illustrated in Fig. 3, the simulations were performed in 2D, assuming plane strain, and the rolling mill was considered as infinitely stiff. Based on [10], the friction coefficient was set equal to 0.3.

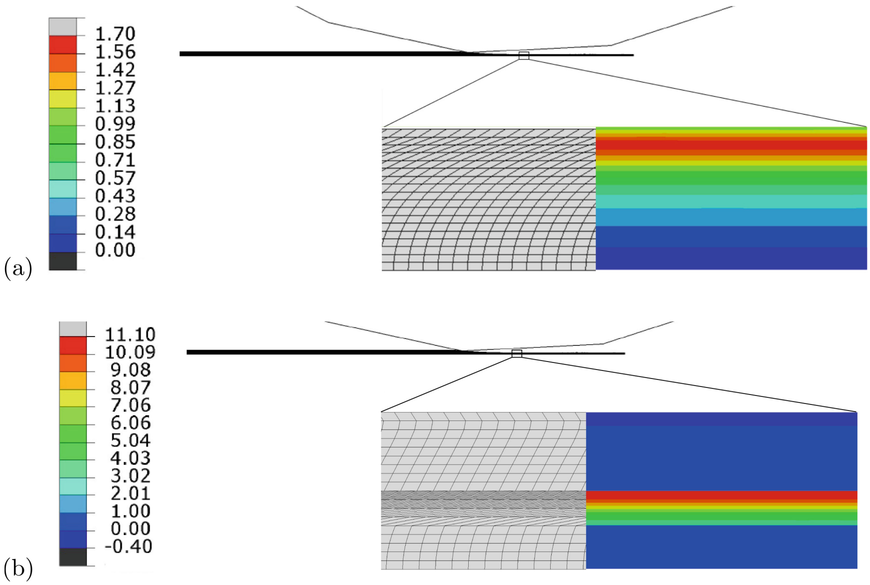

Fig. 3. Heterogeneity of shear (RD-ND component of the deformation gradient tensor) across the half-thickness of the rolled shear. The broken line on the top is the (cylindrical!) rolling mill having a diameter ∼100 times larger than the sheet thickness. The half-thickness shows (a) only Fe (b) one AL1050 layer and two Fe layers.

The sheet thickness was reduced from 1.02 mm to 0.62 mm, corresponding to the second rolling pass in the experiment. Conforming to the laboratory experiment, the rolling draught was large, i.e. the contact length (between roll and sheet) was more than ten times larger than the (aggregate) sheet thickness. The half sheet-thickness was represented by 31896 quadrilateral first order elements.

Two variants of the simulation were carried out. In the first case, we assigned to all finite elements the Armco Iron properties (thus corresponding to traditional rolling). In the second case, a layer of finite elements were assigned properties corresponding to AA1050. The laminated structure then corresponded to the 5-layer samples which had been roll-bonded in the laboratory. The bonding itself was not simulated: the interface between the two materials was tied from the onset of the simulation. In the FE simulation, the material response was considered isotropic (J_2 elasto-plasticity) with a power-law hardening law. As shown in Fig. 3, when the aluminium layer is present, the shear deformation due to the contact with the rolls tends to be concentrated within the aluminium layer instead of spreading across the whole sheet thickness.

Crystal plasticity (CP) theory then allowed predicting the development of texture corresponding to the strain heterogeneity predicted by FE across the sheet thickness. Dislocation slip occurred along $\{111\}\langle110\rangle$ slip systems in the AA1050 layer (fcc), whereas the $\{110\}\langle111\rangle$ and $\{112\}\langle111\rangle$ systems were active in Fe (bcc). The power-law strain hardening maintained an identical critical resolved shear stress (CRSS) on all slip systems. The initial random texture was represented by 1000 grains which were considered to interact in pairs according to the ALAMEL model [11–13]. In Fig. 4, the simulated textures are presented in the form of $\langle111\rangle$ poles figures similar to those presented in Fig. 2. The surface layer made of iron was disregarded as the experimental texture was very weak. In order to check the effect of intense localized shear in AA1050, the simulation of the AA1050 texture was performed twice: either with or without RD-ND shear superimposed to the 75% thickness reduction under plane strain.

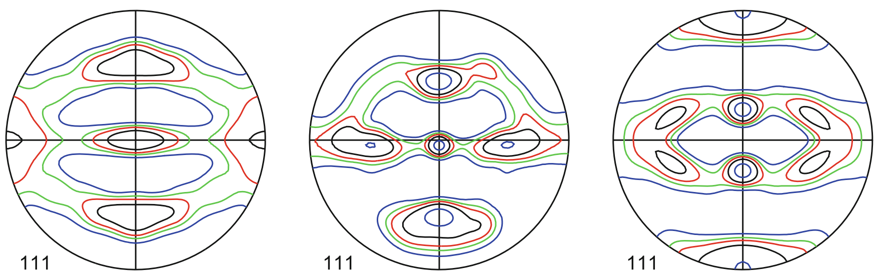

(a) Fe (centre) (b) AA1050 (c) AA1050 (no shear)

Fig. 4. $\langle111\rangle$ poles figures predicted in the central Fe layer (a) and in the AL1050 layer when either using the strain predicted by FE (b) or suppressing the RD-ND shear (c). The contour levels are 0.5/1/1.5/2/5.

The orientation distribution function (ODF) allows a more accurate comparison of the predicted textures to the experimental ones. After rolling of cubic metals, the most relevant information lies in the $\varphi_2 = 45°$ section of the ODF. Figure 5 confirms that crystal plasticity theory provides valid predictions of the texture development in the central Fe layer and in the AA1050 layer on the condition that localized shear within the latter layer is accounted for.

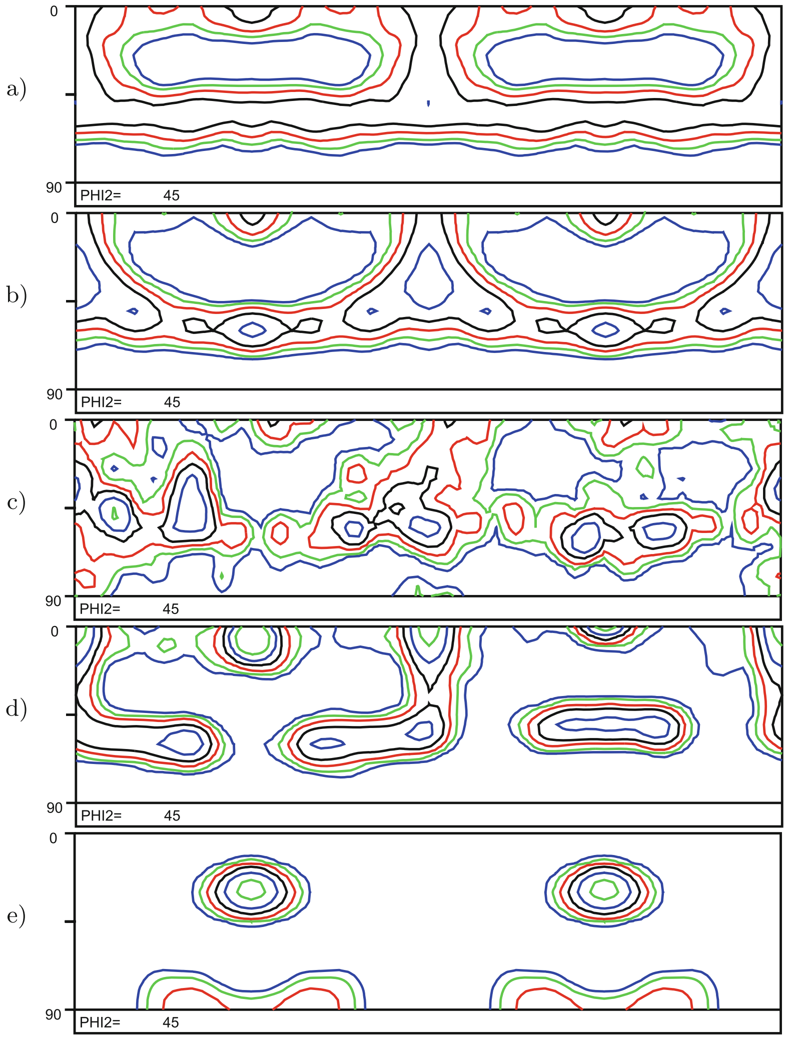

Fig. 5. $\varphi_2 = 45°$ section of the ODF allowing a quantitative assessment of the experimental (a) and predicted (b) textures in the central Fe layer. The experimental (c) texure in AA1050 is compared to predictions which either use the strain predicted by FE (d) or suppress the RD-ND shear (e). The contour levels are 0.5/1/2/4/8.

4 Discussion

Orientation mapping (based on EBSD measurements) is a powerful experimental technique which allowed us to probe both the texture and the microstructure in the different layers of the multilaminate (Fig. 2). However, the technique does not provide direct measurements of the microscopic strain field (unless it is combined with DIC e.g. [14]).

The present work demonstrates the possibility to assist the interpretation of EBSD by relying on numerical modeling (FE and CP). It is only through the combined use of all techniques that we are able to confirm that the AA1050 layer underwent intense shear, causing continuous recrystallization as well as the development of an unconventional texture after cold rolling.

Numerical models also provide estimates of the level of internal stresses, which are at the origin of damage, as well as the plastic anisotropy at the polycrystalline scale. Investigating this in the Fe-Al multilaminate is still ongoing.

It is noteworthy that CP modeling was carried out here in post-processing of the FE modeling which had assumed isotropic mechanical response. This sounds valid because the strain path inside the roll gap is not likely to depend much on plastic anisotropy. When modeling other metal forming processes, such as press forming of metal sheets, a direct micro-to-macro modeling is advisable e.g. [15].

5 Conclusions

- Folding one sheet around the other prior to roll-bonding allowed achieving the production of a 5-layer multilaminate made of ARMCO iron and AA1050.
- The central Fe layer developed a conventional cold rolling texture whereas texture development was slower in the surface Fe layer.
- EBSD measurements in the AA10150 layer revealed a highly refined and equiaxed microstructure, which is indicative of continuous recrystallization.
- According to FE simulations, the soft AA1050 layer hosted intense shear parallel to the rolling plane.
- The comparison of experimental textures to the predictions of CP modeling allowed us to convincingly link the EBSD observation of the different layers to the through-thickness strain heterogeneity predicted by FE modeling.

Acknowledgements. The authors thank Dr. Fengxiang Lin for her advice in the interpretation of EBSD maps. Financial support for this work was provided by the Fonds de la Recherche Scientifique de Belgique (F.R.S.-FNRS). Laurent Delannay is mandated by FSR-FNRS. Computational resources were provided by the Consortium des Équipements de Calcul Intensif (CÉCI), funded by FRS-FNRS under Grant No. 2.5020.11 and by the Walloon Region.

References

1. Nizolek, T., Mara, N.A., Beyerlein, I.J., Avallone, J.T., Scott, J.E., Pollock, T.M.: Processing and deformation behavior of bulk Cu-Nb nanolaminates. Metall. Microstruct. Anal. **3**, 470–476 (2014)

2. Kim, K.J., et al.: Formability of AA5182/polypropylene/AA5182 sandwich sheets. J. Mater. Process. Technol. **139**(1–3), 1–7 (2003)
3. Schoenfeld, S.E., Asaro, R.J.: Through thickness texture gradients in rolled polycrystalline alloys. Int. J. Mech. Sci. **38**(6), 661–683 (1996)
4. Engler, O., Tomé, C.N., Huh, M.Y.: A study of through-thickness texture gradients in rolled sheets. Metall. Mater. Trans. A. **31**(9), 2299–2315 (2000)
5. Tamimi, S., Gracio, J.J., Lopes, A.B., Ahzi, S., Barlat, F.: Asymmetric rolling of interstitial free steel sheets: microstructural evolution and mechanical properties. J. Manuf. Process. **31**, 583–592 (2018)
6. Sidor, J., Petrov, R.H., Kestens, L.: Texture control in aluminum sheets by conventional and asymmetric rolling. Compr. Mater. Process. **3**, 447–498 (2014)
7. Mishin, O.V., Bay, B., Jensen, D.J.: Through-thickness texture gradients in cold-rolled aluminum. Metall. Mater. Trans. A **31**, 1653–1662 (2000)
8. Zhang, Y.B., Mishin, O.V., Godfrey, A.: Analysis of through-thickness heterogeneities of microstructure and texture in nickel after accumulative roll bonding. J. Mater. Sci. **49**, 287–293 (2014)
9. Humphreys, F.J., Hatherly, M.: Recrystallization and Related Annealing Phenomena. Elsevier, Amsterdam (2012)
10. Tieu, A.K., Liu, Y.J.: Friction variation in the cold-rolling process. Tribol. Int. **37**(2), 177–183 (2004)
11. Delannay, L., Mishin, O.V.: Crystal plasticity modeling of the through-thickness texture heterogeneity in heavily rolled aluminum. In: Key Engineering Materials, vol. 554, pp. 1189–1194. Trans Tech Publications Ltd. (2013)
12. Dancette, S., Delannay, L., Renard, K., Melchior, M.A., Jacques, P.J.: Crystal plasticity modeling of texture development and hardening in TWIP steels. Acta Mater. **60**, 2135–2145 (2012)
13. Delannay, L., Tacq, J., Bardel, D., Seefeldt, M.: Direct micro-to-macro modelling of the cold rolling of pearlitic steel. In: MATEC Web of Conferences, vol. 80, p. 02008 (2016)
14. Lin, F.X., Shi, Q., Delannay, L.: Microscopic heterogeneity of plastic strain and lattice rotation in partially recrystallized copper polycrystals. Int. J. Solids Struct. **184**, 167–177 (2020)
15. Delannay, L., Beringhier, M., Chastel, Y., Loge, R.E.: Simulation of cup-drawing based on crystal plasticity applied to reduced grain samplings. Mater. Sci. Forum **495–497**, 1639–1644 (2005)